


# Synthesis of highly dispersible IZO and ITO nanocrystals for the fabrication of transparent nanocomposites in UV- and near IR-blocking

Shaojuan Luo  · Jifei Zou · Hao Luo · Jiyun Feng · Ka Ming Ng

Received: 29 December 2017 / Accepted: 19 March 2018 / Published online: 28 March 2018  
© Springer Science+Business Media B.V., part of Springer Nature 2018

**Abstract** Indium-doped zinc oxide (IZO) nanocrystals were successfully synthesized via the alcohol-assisted pyrolysis of a mixture of indium stearate and zinc stearate, which were fabricated by the direct reaction between the metals and molten stearic acid at a temperature of 260–270 °C. The ~ 10 nm IZO nanocrystals could be dispersed homogeneously in non-polar solvents such as hexane or chloroform, forming an optically clear solution. Transparent IZO-ITO (indium tin oxide)/polyvinyl butyral (PVB) nanocomposite with 10% IZO and 2% ITO loading shows more than 75% visible light transmittance, 100% UV-blocking (below 380 nm), and 100% blocking of NIR from 1600 to 2500 nm. Equilibrium molecular dynamic simulation results clearly stated

the stearic acid wrapped IZO nanocrystals in PVB matrix would hardly affect the solubility parameter of PVB composite, indicating their good compatibility and guaranteeing the high transparency of PVB-based composites. Our strategy paves the way to facile synthesize non-polar solvent soluble nanocrystals and fabricate transparent PVB-based functional nanocomposite.

**Keywords** IZO nanocrystals · Dispersion · Transparent nanocomposite · UV- and NIR-blocking · Equilibrium molecular dynamic simulation

Shaojuan Luo and Jifei Zou contributed equally to this work.

**Electronic supplementary material** The online version of this article (<https://doi.org/10.1007/s11051-018-4198-2>) contains supplementary material, which is available to authorized users.

S. Luo · J. Zou  
Shenzhen Engineering Laboratory of Phosphorene and Optoelectronics, International Collaborative Laboratory of 2D Materials for Optoelectronic Science and Technology, Shenzhen University, Shenzhen 518060, People's Republic of China

S. Luo (✉) · J. Feng · K. M. Ng (✉)  
Department of Chemical and Biological Engineering, The Hong Kong University of Science and Technology, Clear Water Bay, Kowloon, Hong Kong  
e-mail: kesjluo@connect.ust.hk; e-mail: kekmg@ust.hk

H. Luo  
The National Engineering Research Center of Novel Equipment for Polymer Processing, South China University of Technology, Guangzhou 510640, People's Republic of China

## Introduction

Smart windows have large end-use markets within the architectural (residential and commercial buildings) and transportation (cars, airplanes, boats) sectors, with low-e windows occupying most of the global passive smart window market (NanoMarkets 2014). Low-e glass allows for energy savings in buildings by blocking harmful radiation and heat from sunlight. These passive smart windows with sound, ultraviolet (UV)- and infrared (IR)-blocking properties have drawn considerable interest in their potential applications in green buildings and vehicles (Jiang et al. 2013; Mahltig et al. 2005; Morimoto et al. 1999). They can hinder the damage of ultraviolet rays by blocking all the UV radiation, save energy by reflecting the infrared light and insulate against noise pollution but let the visible light go through. At present, indium tin oxide (ITO) is one of the key materials as an IR-reflecting architectural

coating (Sunde et al. 2012) and a transparent conductive coating (Zhao et al. 2009; Dattoli and Lu 2011). In our previous work, we successfully synthesized dispersible ITO nanocrystals and integrated ITO into polyvinyl butyral (PVB) film to prepare NIR-blocking nanocomposites (Luo et al. 2014b).

A great deal of recent research has been focused on the development of different method to protect matter from harmful UV radiation including both UVB and UVA radiation. The inorganic and organic UV-absorbing agents can be used to protect against UV radiation, the organic UV-absorber molecules including a phenolic group play an important role in the dissipation of the absorbed energy (Zayat et al. 2007), while the inorganic UV-protective materials mainly base on band-gap semiconductors ZnO, TiO<sub>2</sub>, and CeO<sub>2</sub> to attenuate UV radiation by absorbing or scattering light (Lee 2009; Becheri et al. 2008; Zhang and Han 2016; Tao et al. 2016; Lizundia et al. 2016; Shaheen et al. 2016). However, pure ZnO has a cut-off point of about 360 nm (Sun et al. 2008; Khrenov et al. 2005). Based on the Moss-Burstein effect (Hammarberg et al. 2009), a doped ZnO is expected to possess a larger band-gap and improves the UV-blocking performance. Moreover, a high transmittance is a prerequisite for using doped ZnO in an optical nanocomposite; thus, the particles must be integrated in a way leading to isolated primary particles inside the polymer matrix without agglomeration and complements ITO's lack of UV-blocking. Conventionally, doped ZnO nanocrystals are synthesized in solution, employing chemical precursors in the form of acetates (Lee and Park 2003; Olvera et al. 2007; Wienke and Booij 2008), chlorides (Chen et al. 2010; Lee et al. 2003), nitrates (Kim et al. 2009; Al Dahoudi et al. 2013), or acetylacetonates (Raj et al. 2008; Maldonado et al. 2004). In all of these cases, aggregation of the particles is a common problem. Some researchers turned to use the long alkyl chain organometallic precursors to obtain monodisperse-doped ZnO nanocrystals (Wang et al. 2010; Chen et al. 2005). IZO has been well-studied, demonstrating superior optoelectronic properties as TCO material; in addition, both zinc oxide and indium oxide nanocrystals are readily synthesized by one-step ester elimination reaction based on pyrolysis of metal carboxylate salts (Chen et al. 2005; Luo et al. 2013). Along a similar direction, we developed a novel, one-pot pyrolysis method to fabricate indium and zinc stearate, which were applied to synthesize high quality indium-doped zinc oxide (IZO) and

ITO that can be readily dispersed in non-polar solvent. The transparent nanocomposite IZO-ITO/PVB with UV and near-IR double-blocking function was fabricated via the film casting method. Meanwhile, equilibrium molecular dynamic simulation was performed to simulate the dissolution behaviors of wrapped surfactant of nanocrystals and PVB polymer matrix.

## Experimental details

### Chemicals

Raw indium metal (indium ingot, 99.995%), zinc metal (zinc powder, 98%), and tin metal (tin granules, 99.999%) were purchased from Zhuzhou Smelter Group Co., Ltd., PRC; stearic acid (95%), oleyl alcohol (85%), and PVB resin were obtained from Sigma-Aldrich Company; chloroform (99.8%) and ethanol (99.9%) were from Merck. All the chemicals were used as received without any further purification.

### Synthesis of indium and zinc stearate precursors

0.01 mol of zinc metal and 0.021 mol of stearic acid were introduced into a 50-mL condenser-equipped three-neck round-bottom flask. The raw materials were heated to 270 °C and maintained at this temperature with vigorous stirring under nitrogen flow. The stearic acid was in molten state, and some bubbles came out from the reaction solution. After 5 h, zinc metal almost disappeared, indicating that zinc reacted with stearic acid, and formed an optically clear solution with brown color. Subsequently, the as-synthesized zinc stearate precursor in waxy solid form was obtained by cooling the solution to room temperature for characterization of the precursor. Depending on the desired indium doping level, for example IZO-10%, a certain amount (0.965 g) of indium stearate (prepared in a similarly manner (Luo et al. 2013; Luo et al. 2014a, b) was added into the flask and mixed with the zinc stearate by magnetic stirring at 150 °C. After about 15 min, a homogeneous solution was obtained, and the indium-zinc stearate precursor in solid form can be achieved by cooling the solution to room temperature. Hereby, the designed indium doping levels of mix precursor were from 2 to 15% in this experiment.

## Synthesis of IZO and ITO nanocrystals

The indium-zinc stearate precursor was heated from room temperature to 270 °C at a heating rate of 10 °C/min. When the temperature reached 270 °C, 8.6 mL (0.023 mol) oleic alcohol (85%, Sigma-Aldrich) was quickly injected to the flask. The reaction maintained at 270 °C for the pyrolysis reaction under a nitrogen atmosphere. After 3 h, the flask was cooled down and a green precipitate was obtained. Then, the precipitate was washed by hot ethanol to remove the by-products, and dried at 70 °C overnight. Finally, the IZO nanocrystals in powder form were obtained. The IZO samples are labeled as IZO-x%-270, where x indexes the indium doping level. The IZO-10%-270 nanocrystals were dispersed in chloroform forming light green optically clear solution, while the ITO nanocrystals were synthesized in a same way as report (Luo et al. 2014b). A light blue optically clear ITO chloroform solution could be obtained at the same time.

## Preparation of IZO-ITO/PVB nanocomposite

1.0 g of PVB, 1 mL of ITO chloroform solution (20 mg/mL), and certain amount of IZO chloroform solution were added into 10 mL of chloroform and vigorously stirred to obtain homogenous PVB solutions containing IZO (from 1 to 10%) and 2% ITO nanocrystals at room temperature (all the loading percentage is weight percentage). 1.5 or 3.0 mL of the prepared solutions were poured into the glass petri dishes (30 mm in diameter) carefully without forming bubbles. The petri dishes were transferred to a flat fume hood, after the solvent evaporated completely, transparent IZO-ITO/PVB nanocomposite films were obtained and could be carefully peeled from the petri dishes. The thickness of these films was measured by a digital caliper. Figure 1 illustrates the fabrication process of a transparent nanocomposite film.

## Characterization

Thermogravimetric analysis (TGA) was performed on a TGA (Perkin Elmer, UNIX/TGA7) from room temperature to 700 °C in an air atmosphere with a heating rate of 10 °C/min. Fourier transform infrared spectrum (FT-IR) of the zinc stearate precursor was obtained by using an FT-IR spectrometer (Bio-Rad, FTS6000) with attenuated total reflection (ATR) mode. Phase

identification and structural analysis of the IZO nanocrystals were conducted on a Phillips X'pert Pro X-ray diffractometer equipped with Cu K $\alpha$  radiation ( $\lambda = 1.54056 \text{ \AA}$ ) at a scan rate of 0.5°/s and  $2\theta$  from 10° to 70°, operating at 40 kV and 40 mA. X-ray photoelectron spectroscopy (XPS, Axis Ultra DLD) were applied to characterize elemental composition and chemical state of the IZO nanocrystals. Electron micrographs of the IZO nanocrystals were taken using a high-resolution transmission electron microscope (HRTEM) (JEOL-2010F) with an accelerating voltage of 200 kV, equipped with selected area electron diffraction (SAED). TEM observation of the distribution of nanocrystals in PVB matrix was conducted on a transmission electron microscope (TEM) (JEOL 100CX) operating at an accelerating voltage of 100 kV. The nanocomposite samples were prepared by dropping a drop of the IZO-ITO/PVB chloroform solution onto the water surface using the 50- $\mu$ L pipette tip. A very thin layer of film was formed, and it could be captured by a carbon layer coated copper grid. UV-Vis spectra of the nanocomposites were recorded by a UV-Vis spectrometer (UV-1700, Shimadzu) using a transmission mode, and the wavelength scan range is from 300 to 800 nm. Near IR spectra were recorded by FT-NIR spectrometer (Bruker, Vertex70), and the wavelength ranges from 900 to 2500 nm. TOF-SIMS analysis of the IZO nanoparticle surface was performed on TOF SIMS V (ION-TOF GmbH), and a Cs<sup>+</sup> source was used.

## Calculation details

Equilibrium molecular dynamic (EMD) simulation was performed by means of Forcite module in Materials studio® 5.0 to simulate the dissolution behaviors of stearic acid in PVB. The structure of PVB chain (used X<sub>80</sub>Y<sub>18</sub>Z<sub>2</sub> as simulation model, see Fig. S1) was optimized under the following convergence criteria:  $2.0 \times 10^{-5}$  kcal/mol for energy, 0.001 kcal/mol/Å for force, and  $1.0 \times 10^{-5}$  for displacement. After the geometry optimization, EMD calculation with NVT ensemble and Universal force field (UFF) (Rappe et al. 1992) was performed at time step of 1.0 fs up to total 5.0 ns, among which Andersen algorithm thermostat with 1.0 Collision ratio was used to maintain the temperature of the system at around 298 K.

The cohesive energy density (CED) was defined as Eq. 1, where  $\Delta H$  is heat of evaporation. Since high molecular polymer usually decomposes before it

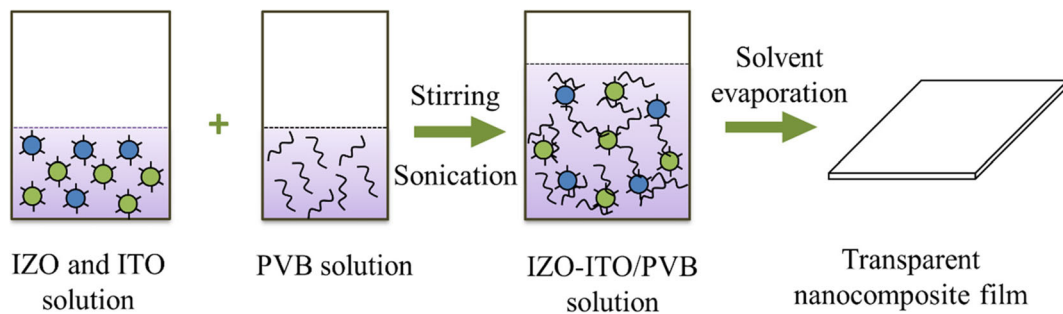


**Fig. 1** Schematic diagram of the fabrication process of transparent nanocomposite with UV- and near-IR double-blocking function

evaporates, the CED are often calculated with group contribution methods (Li et al. 1997)

$$\text{CED} = \frac{\Delta H - RT}{V_m} \quad (1)$$

$$\delta = \sqrt{\text{CED}} \quad (2)$$

whereas the solubility parameter  $\delta$  was defined as the square root of CED (see Eq. 2).

## Results and discussions

### Identification of the zinc stearate precursor

Zinc stearate precursor was successfully synthesized via the direct reaction process. The Fourier transform infrared spectrum of the zinc stearate shows 1 asymmetric  $\text{COO}^-$  stretching peaks ( $1527 \text{ cm}^{-1}$ ) of zinc carboxylate groups from  $1510$  to  $1630 \text{ cm}^{-1}$  which are the characteristic peaks different from the neat stearic acid (Fig. 2a). Moreover, clear weakening of the  $-\text{OH}(\delta)$  stretching peak at  $943 \text{ cm}^{-1}$ , and  $-\text{COOH}(\delta)$  stretching peak at  $1294 \text{ cm}^{-1}$  implied that the formation of zinc carboxylate. The spectrum of the product is similar with the standard pattern (SDBS #3130), and it can be confirmed as zinc stearate. As described in the experimental section, the indium-zinc stearate was fabricated by mixing up indium stearate and zinc stearate which is different from the indium-tin stearate (Luo et al. 2014a, 2015; Dou and Ng, 2016). It is interesting that the indium and tin alloy metals can react with stearic acid completely and form indium-tin stearate, while the yield of indium-zinc stearate is only about 25% using indium and zinc mix-metals reacted with stearic acid at the same

time; furthermore, the same result was obtained when zinc was replaced by gallium metal (see Table S1 in the supporting information). Up to our knowledge, the explanation of the phenomenon has not been confirmed yet. We assume that the reaction in indium-tin system is synergic, while the reactions in indium-zinc systems are antagonistic.

Figure 2b presents the TGA curve of the precursor, revealing that its pyrolysis mainly occurred at about  $325$ – $400 \text{ }^\circ\text{C}$ . When the temperature reached  $500 \text{ }^\circ\text{C}$ , the weight loss stayed unchanged, illustrating that the precursor zinc stearate had decomposed completely to generate ZnO product. Zinc stearate was found to be more stable with the reaction up to  $320 \text{ }^\circ\text{C}$ , comparing to indium stearate (Luo et al. 2013). As presented in Fig. S2, the well-mixed indium-zinc stearate precursors with different In doping levels have similar tendency, the dramatic decline of weight loss mainly concentrated at about  $350$ – $425 \text{ }^\circ\text{C}$ , as the amount of indium stearate increases, the main pyrolysis temperature would decrease at the same time. As a result, the size of the particle would decrease according to the previous experience. We deduce that the reactivity of the indium stearate is higher than that of zinc stearate. Thus, the zinc stearate accounts for the main pyrolysis reaction during the synthesis process.

### Synthesis of IZO nanocrystals by alcohol-assisted pyrolysis

There is a kinetically energy barrier between the reactants and products, because the nanocrystals are thermodynamic metastable species (Chen et al. 2005; Mozaffari et al. 2017). For the pyrolysis reaction, we tried to increase the pyrolysis temperature to overcome the kinetic barrier; as a result, the particles kept on growing and leading to a large particle size. With the

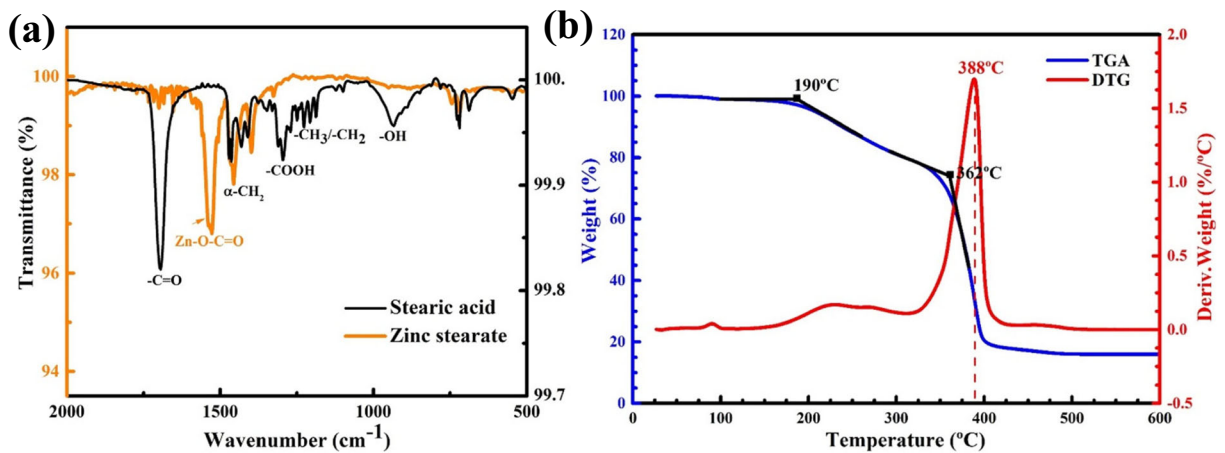


**Fig. 2** **a** FT-IR spectra of the stearic acid and zinc stearate. Orange curve: zinc stearate. Black curve: stearic acid. The assignments of the main IR vibration bands of the spectra are also shown. **b** TGA

and DTG curves of zinc stearate. The displayed temperatures 190 and 362 °C are the estimated nucleation and main growth temperatures, respectively

purpose of synthesis of IZO nanocrystals, oleyl alcohol was applied to the reaction as an additive to lower the kinetic barrier by esterification. The  $-OH$  group nucleophilically attacks the carboxylates ( $-C=O$ ) to form an ester, accelerating the formation of IZO at a relatively low reaction temperature. During the alcoholysis, the by-products (Oleic compounds) after esterification served as solvent/surfactant to dilute the concentration of the nuclei and promote the formation of monodisperse IZO nanocrystals. The reaction temperature can be lowered down owing to the nucleophilically attack (comparing with the TGA curves in Fig. S2), but the lower temperature would lead to low reactivity and result in poor crystallinity. Thus, the temperature selection is a key factor in the synthesis process. Another parallel experiments were conducted at the temperatures of 300, 250, and 200 °C for 3 h, and the corresponding TEM images of the obtained products are illustrated in Fig. S3. When the pyrolysis took place at 300 °C, the obtained product IZO-10%-300 was almost monodisperse but with the relative large size. In Fig. S3c, some tiny crystals can be found in the TEM image, it means the reactivity is low and the particles need a long time period to grow. The amorphous-like IZO-10%-200 sample indicates the reaction almost cannot happen at this temperature. From an engineering aspect, we choose 270 °C as the operation temperature to synthesize the IZO nanocrystals.

The XRD pattern of IZO nanocrystals is displayed in Fig. 3. The peaks centered at the peak positions match quite well with the main diffraction peaks of the

hexagonal wurtzite zinc oxide (JCPDS#36-1451), and no peaks of discernable indium oxide or other zinc oxide compounds were detected. Along with the increase of indium dopant level, the peaks become weaker and boarder, elucidating the decreased size of the IZO nanocrystals according to the Debye-Scherrer equation. No other peaks of impurity were found even in the IZO-15%-270 sample, which promised the well distribution of indium ions in the zinc oxide lattices. The ionic radii of  $Zn^{2+}$  and  $In^{3+}$  are 0.074 and 0.080 nm, respectively, which imply little lattice distortion in the IZO nanocrystals while indium inserting to the zinc oxide lattice. Thereby, the alcoholysis of well-mixed indium-

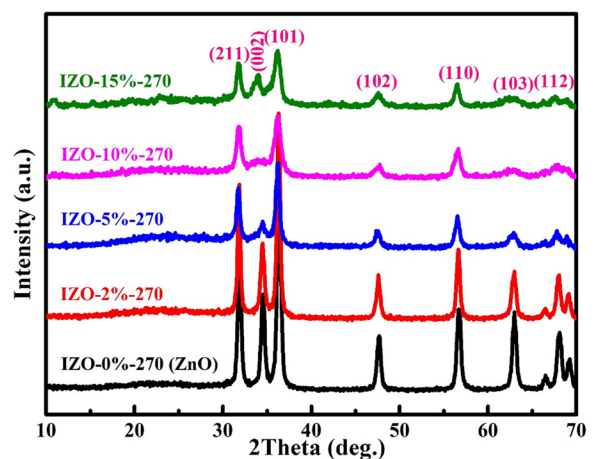


**Fig. 3** XRD patterns of IZO nanocrystals with different indium doping levels. Standard patterns of hexagonal wurtzite ZnO (JCPDS #36-1451) are also listed

zinc stearate explores an efficient way to synthesize the IZO nanocrystals with a wide range of indium doping levels.

Figure 4 presents the XPS spectra of IZO-10%-270 nanocrystals. From the survey spectrum shown in Fig. 4a, it could be found that the elements of zinc (Zn 2*p*), indium (In 3*d*), oxygen (O 1*s*), and carbon (C 1*s*) were detectable, elucidating no obvious impurities were introduced. The appearance of C 1*s* core-level indicates the grafted fatty acid attaches on the surface of IZO nanocrystals comparing to the pure IZO sample (Chava and Kang 2017). The spectrum of O 1*s* was fitted by two deconvoluted Gaussian peaks which were located at 530.9 and 532.4 eV, the peak located at 530.9 eV corresponds to the Zn–O bonding, while the higher binding energy centered at 532.4 eV belonged to

O and O<sub>2</sub> ions in the oxygen-deficient region caused by oxygen vacancies as In<sup>3+</sup> cations insert the zinc oxide lattices (Chen et al. 2011). Figure 4c, d shows the peaks of zinc and indium, the observed binding energy peaks of Zn 2*p* at 1021.8 and 1044.9 eV could be assigned to ZnO and the binding energies of In 3*d*<sub>5/2</sub> and In 3*d*<sub>3/2</sub> were at 445.2 and 452.8 eV, respectively, corresponding to In<sub>2</sub>O<sub>3</sub> (Beena et al. 2009). The energy difference for two Zn 2*p* was 23.1 eV and for two In 3*d* peaks was 7.6 eV, which matches well with the standard value of 22.97 and 7.5 eV (Chava and Kang 2017), suggesting the valence states of Zn and In ions to be Zn<sup>2+</sup> and In<sup>3+</sup>, respectively. These results were consistent with the XRD characterization. At the same time, the XPS analysis (Table 1) shows that the atomic In to Zn ratio of IZO nanocrystals was 10.3% which is consistent with the

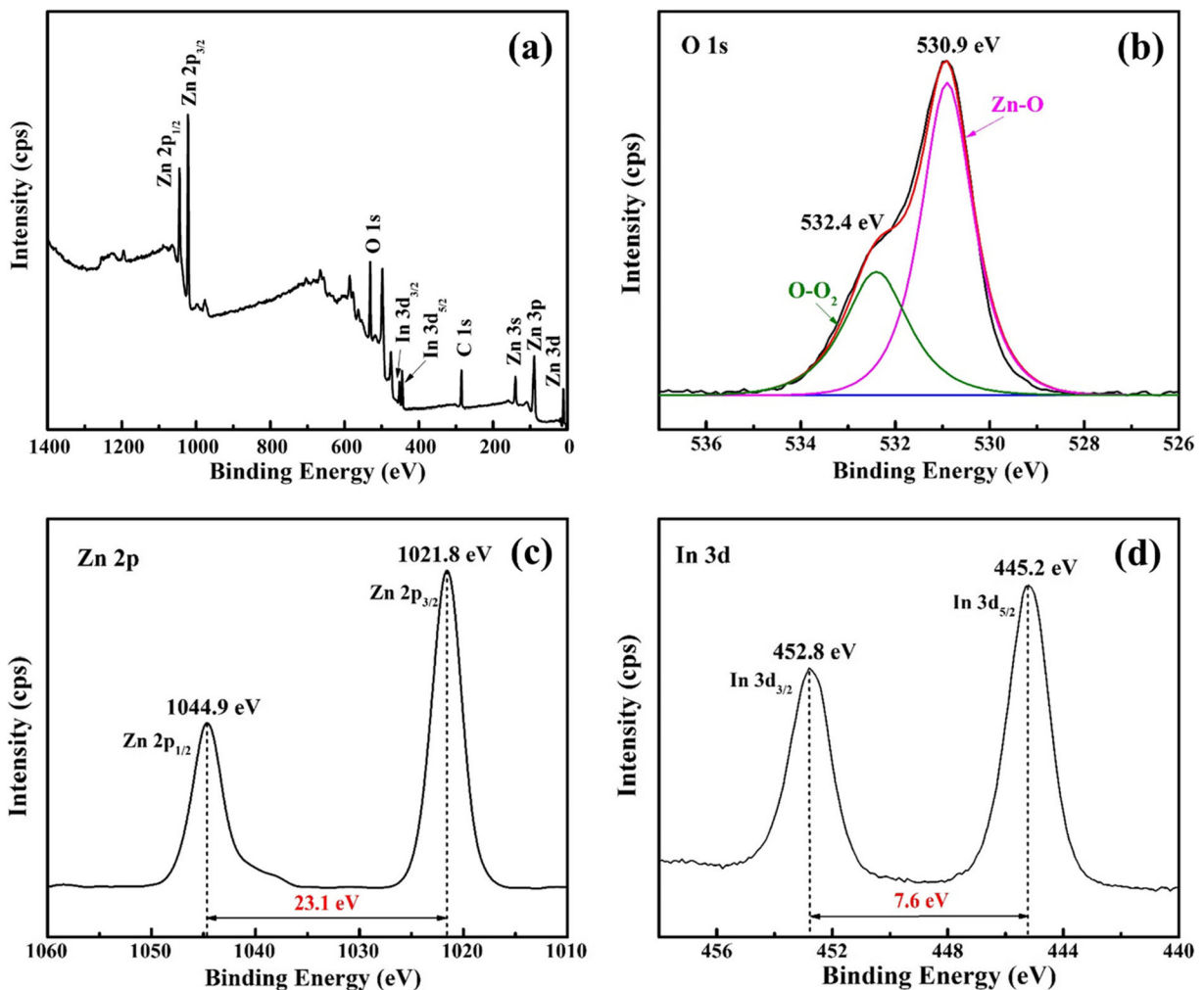


**Fig. 4** XPS spectra of IZO nanocrystals. **a** Survey spectrum. **b** Narrow scan of O 1*s*. **c** Narrow scan of Zn 2*p*. **d** Narrow scan of In 3*d*

**Table 1** XPS quantification report of the IZO nanocrystals

Peak	O 1s	Zn 2p	In 3d	C 1s
Atomic conc.%	36.54	23.84	2.45	37.17
Mass conc.%	20.36	54.3	9.79	15.55

initial In/Zn ratio (10%) used in this sample. The result indicated that the indium ions inserted into the zinc oxide lattice and formed indium-doped zinc oxide; therefore, the IZO nanocrystals consist of a solid solution of the indium-zinc oxide.

The monodispersed IZO-10%-270 nanocrystals were successfully synthesized and existed in particle form without any agglomerations (Fig. 5a), the high-resolution TEM image (Fig. 5b) depicts the particles are single crystalline with a lattice spacing of 0.276 nm from the [100] planes. The XRD results are further confirmed by the TEM observations as shown in Fig. S4(a–c), as In doping levels increases from 5 to 15 wt%, and the average particles size of the corresponding IZO nanocrystals decreases from 27 to 10.5 nm. The IZO samples can be dispersed in the non-polar solvent such as hexane, toluene, or chloroform to form optically clear solution, a photo of IZO chloroform dispersion is illustrated in Fig. 5a inset (also in Fig. S4d). The result indicates that the IZO crystals prepared with this method could be dispersed homogeneously in the non-polar solvent.

TOF-SIMS technique was applied to study the surface of the as-synthesized IZO nanocrystals. Figure S5 shows the positive and negative TOF-SIMS spectra of the IZO surface, and the fragments such as  $C_{16}H_{31}O_2$  and  $C_{18}H_{35}O_2$  were detected. The fragments comprised  $-COO^-$  groups and long hydrophobic chains, which attached to the surface of IZO as stabilizers, this self-assembly organic layer wrapped the IZO nanocrystals leading to excellent dispersity of the IZO nanocrystals in non-polar solvents. The steric hindrance of the grafted fatty acid molecule layers was produced during the alcoholysis of the organo-metallic precursors to form IZO nanoparticles, which is in accordance with the XPS results. PVB was found to stabilize the fatty acid dispersion (Kirchberg et al. 2012; Rudolph and Peuker 2011); consequently, the strong chemical interaction between the polymeric matrix and fatty acid coated IZO could be expected, resulting in IZO nanocrystals were uniformly surrounded by the polymeric matrix PVB. To determine the amount of stabilizers on the surface of IZO nanoparticles quantitatively, TGA was utilized. Figure S6 depicts the TGA curves of the IZO nanoparticles as well as stearic acid under nitrogen atmosphere. The weight loss of the as-synthesized IZO include three processes: in the first step (below 120 °C), the weight loss was due to the water evaporation; in the second step (120–550 °C), the main weight loss concentrated in this temperature region, while the main weight loss of stearic acid happened at 120–250 °C.

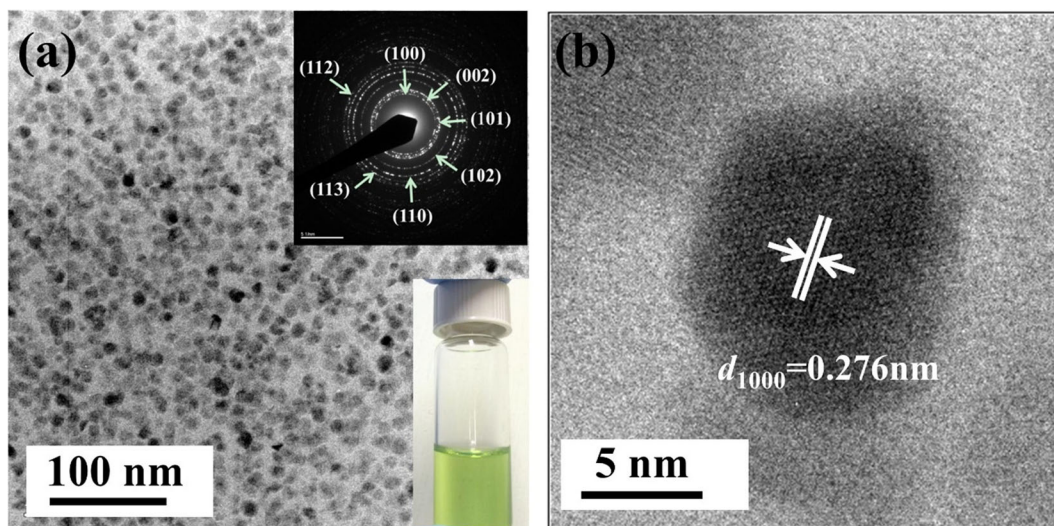


**Fig. 5** a Low-resolution and b high-resolution TEM images of the IZO-10%-270 nanocrystals. The SAED pattern and photograph of IZO in chloroform solution are shown as insets in a

The obvious difference may be due to the existing status of the stearic acid. Free stearic acid is easier to decompose than the adsorbed one, because more kinetic barriers need to overcome on account of chemical adsorption. The last step, the weight loss stayed changed since the temperature reached 600 °C, illustrating that the stabilizers were removed completely. From the TGA curve, it is estimated that the amount of the stabilizers on the surface of the IZO nanoparticles is about 10 wt% with respect to the total weight of the as-synthesized IZO nanoparticles. Accordingly, the presence of the stabilizers on the surface of the as-synthesized IZO nanoparticles makes them also meet the condition to prepare transparent composite materials.

### Optical properties of the nanocomposites

In order to study the distribution of IZO and ITO nanocrystals in PVB matrix, TEM was used. Figure 6 shows the TEM image of IZO and ITO nanocrystals distributed in PVB matrix. Clearly, the TEM image shows that the IZO and ITO nanocrystals are homogeneously dispersed in PVB matrix as we expected. The nanocrystals are present in single particle form in the PVB matrix. Although we cannot distinguish IZO and ITO nanocrystals owing to the low resolution, this TEM image indeed provide a visual evidence of the homogeneously dispersion of nanocrystals in polymer matrix.

With increase in UV radiation dosage (including both UVB and UVA radiation), the rate of photo injury

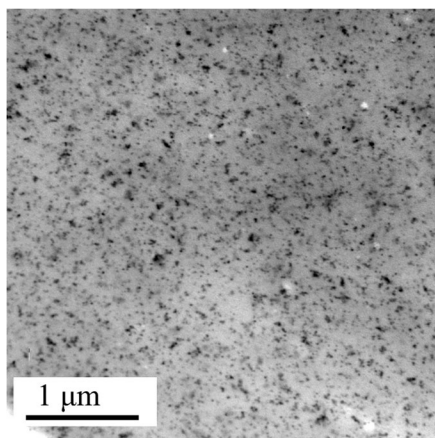


**Fig. 6** TEM image of IZO and ITO nanocrystals distributed in PVB matrix (samples 10%IZO-2%ITO/PVB)

resulting from hazardous UVB emission increased by 12% during the period from 1988 to 1999, as compared with the rate during the earlier years of the decade (Li et al. 2006). In addition with the saving concern, a great deal of recent research has focused on the development of materials with good capability of transmission of visible light as well as to block the UV and IR radiation.

Figure 7a shows the UV-Vis spectra of IZO chloroform solution with different concentrations. From the curves we can find that, as the concentration increases, the transmittance in visible light range would decrease, but the UV-blocking efficiency is increased significantly. The cut-off points of the UV light of the five dispersions are 370, 382, 395, 403, and 417 nm, respectively. The IZO-10%-270 solution with the concentration higher than 1% would block 100% UV light according to our study (the testing light path is 1 cm). The result shows the IZO solution preforms much better in UV absorption than the traditional ZnO whose cut-off point is 360 nm (Sirvio et al. 2016; Shaheen et al. 2016; Lizundia et al. 2016; Sun et al. 2008; Khrenov et al. 2005). For a doped zinc oxide, owing to the higher concentration of free charge carriers, the partial filling of the conductance band is well-known as the Möss-Burnstein effect (Hammarberg et al. 2009). Therefore, a larger band-gap energy of the IZO sample would be obtained comparing to non-doped ZnO (Fig. S7). The increasing band-gap of IZO nanocrystals may lead to the red shift of cut-off point and increase the UV-blocking performance.

Figure 7b presents the UV-VIS spectra of the x%IZO-2%ITO/PVB nanocomposites with different IZO loadings (the thickness of the nanocomposite is 0.12 nm). As it can be seen from the spectra, in the visible light range of 400–800 nm, as IZO the loading increases from 0 to 10%, the transmittance of the composites shows a slightly decrease which is about 5%. However, the transmittance is still about 80%. The slight loss of transmittance of the nanocomposite is consistent with the light scattering particle size according to Rayleigh's law (Althues et al. 2007) due to the excellent homogeneous distribution of the IZO and ITO nanocrystals in the polymer matrix. Transparent IZO-ITO/PVB nanocomposite with 10% IZO loading and 0.24 mm in thickness shows 100% UV-blocking in 380 nm, 90% UV-blocking in 400 nm, and over 75% transmittance in visible light range; this excellent performance exhibits a great potential in many applications.



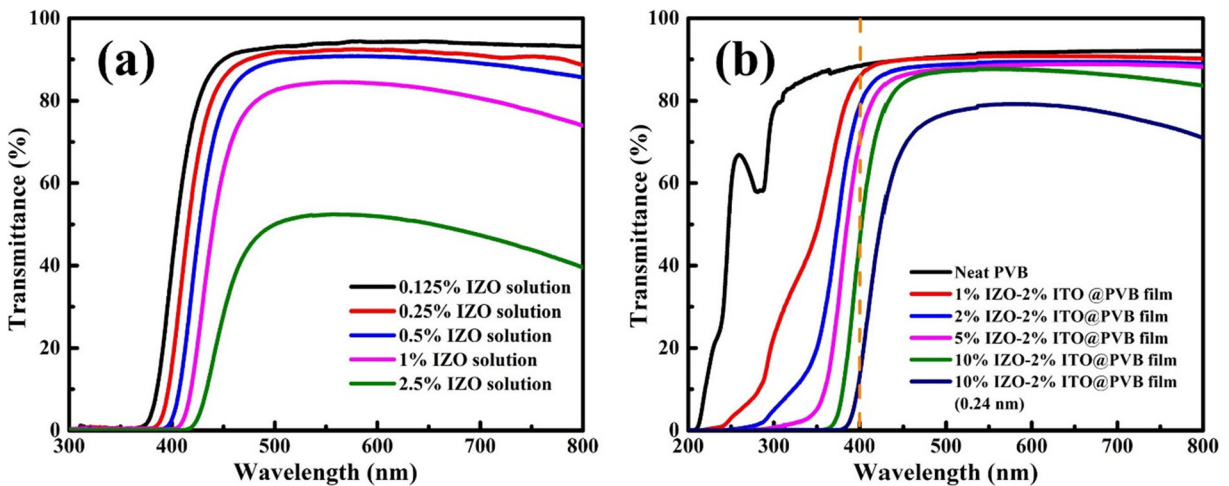


**Fig. 7** UV-Vis spectra of **a** IZO solutions with different concentrations of IZO nanocrystals in chloroform (weight percentage) and **b** IZO-ITO/PVB nanocomposite films with different IZO loadings

FT-IR spectra of four nanocomposite samples are depicted in Fig. 8. As we compare four spectra of the samples, the IZO/PVB composite shows no significant effect in NIR-blocking, although the IZO loading in the PVB matrix is up to 5%. The nanocomposites with 10% IZO and 2% ITO loading depicts nearly 100% IR-blocking from 1600 to 2500 nm, the NIR-blocking effect should mainly attribute to the ITO species. Consequently, as the increase of the composite film thickness, a slight improvement of the NIR shielding performance was observed, not that distinctness. This phenomenon indicates that the highly transparent nanocomposite of 0.12 mm in thickness with 10% IZO and

2% ITO is an excellent UV and near IR blocker (Fig. S8). Moreover, the thickness of the common PVB film used in the industry generally is 0.38 mm, which is three times thicker than our samples. Based on the current experimental results, a propositional formula for practical production is 3.5% IZO and 0.7% ITO loading in PVB, which would lead the 0.38 mm nanocomposite to become a superior UV and NIR shield (Fig. S9).

Theoretical calculation discussion

After the geometry optimization, the energetic-minimized configuration of one molecule of stearic acid dissolving in two PVB chains was shown in Fig. 9a. The calculation model was designed based on our experimental recipe; the composite with 10% IZO in PVB would contain about 1 wt% stearic acid core, 9 wt% IZO, and 90 wt% PVB. For simplification, 1 wt% stearic acid and 99 wt% PVB were designed in the calculation system. Obviously, no cross-linking of these two PVB chains was observed, elucidating stearic acid was compatible with PVB chains and the kept the original properties of PVB. The simulated solubility parameter of pure PVB is about 17.2–17.6 (J/cm<sup>3</sup>)<sup>0.5</sup>, the number is little smaller than the theoretical value of pure PVB of 18.6 (Hansen 2007) owing to the model simplification. After adding 1 wt% stearic acid to the system, the solubility parameter of PVB/stearic acid mixture increases to about 17.7–18.2, the slight change indicates

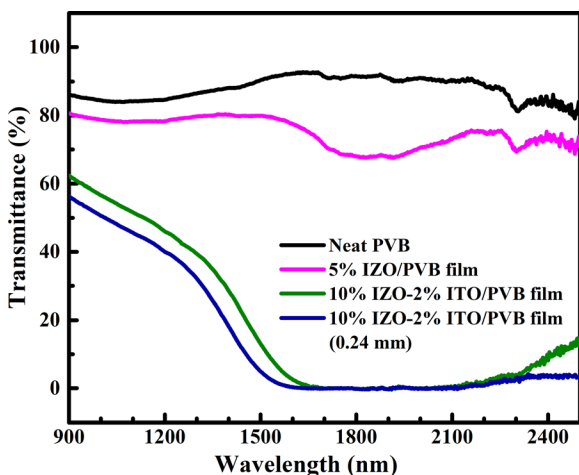


**Fig. 8** FT-IR spectra of neat PVB and 3 pieces of IZO-ITO/PVB nanocomposite films

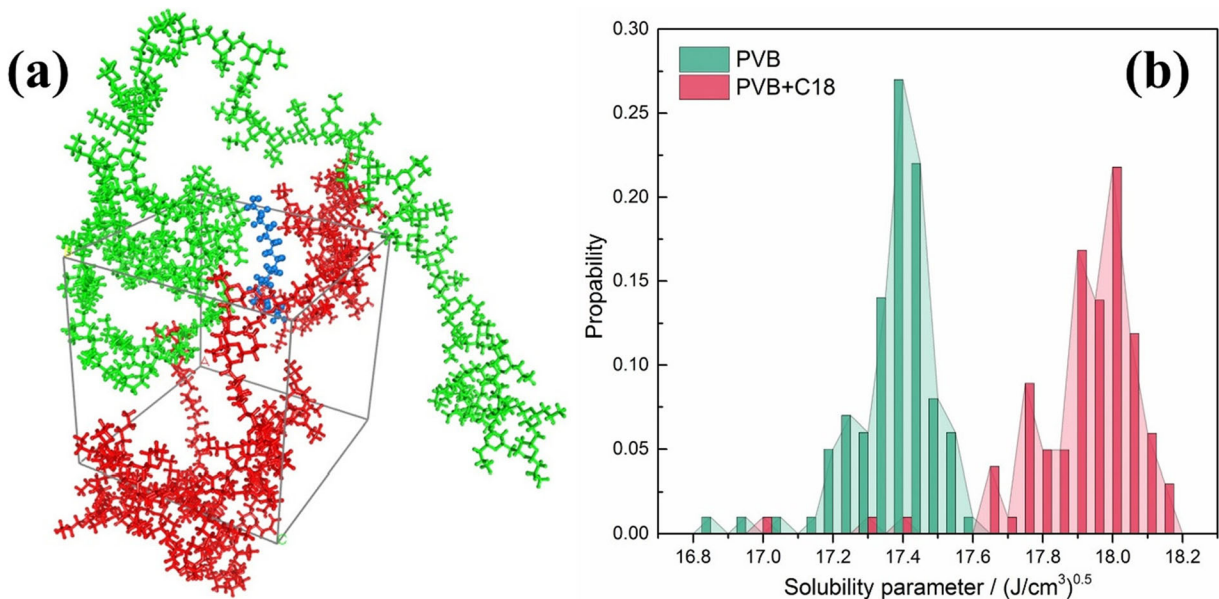


**Fig. 9** **a** The energetic-minimized configuration of one molecule of stearic acid (marked as blue, ~1 wt%) dissolves in two PVB chains (marked as red and green, respectively, ~99 wt%) and **b** solubility parameter of pure PVB and PVB (99 wt%)/ stearic acid (1 wt%) mixture

the good compatibility between stearic acid and PVB. The simulation results clearly stated that good compatibility trend of stearic acid and PVB which ensures the transparency of the PVB-based composite despite the model is simplified. The simulation results were consistent with our experimental outcome.

## Conclusions

In summary, the IZO nanocrystals were successfully synthesized via the alcohol-assisted pyrolysis of the mixture of indium stearate and zinc stearate, which were fabricated by the direct reactions between the metals and molten stearic acid at the temperature of 260–270 °C. The ~10 nm IZO nanocrystals and ~7 nm ITO nanocrystals can be dispersed homogeneously in non-polar solvents such as hexane, toluene, or chloroform, forming the optically clear solution. The IZO chloroform solution with the 1% weight percentage of IZO nanocrystals can block 100% UV light and turn into promising materials as excellent UV light absorber. Transparent IZO-ITO/PVB nanocomposite with 10% IZO and 2% ITO loading shows 75% visible light transmittance, 100% UV-blocking, and 100% near IR-blocking (from 1600 to 2500 nm). Theoretical calculations clearly stated the good compatibility between stearic acid and PVB matrix, guaranteeing the high

transparency of PVB-based composites. As a result, our receipt allows the transparent nanocomposite to become a potential material in many applications.

**Author contributions** S.J. Luo and J.F. Zou contributed equally to this work. The manuscript was written through contributions of all authors. All authors have given approval to the final version of the manuscript. Funding This study is financially supported by the University Grants Council of the Hong Kong Government, Natural Science Foundation of Guangdong Province (2016A030310048), Student Innovation Development Foundation of Shenzhen University (PIDFP-ZR2017023) and China Postdoctoral Science Foundation (2016 M592530). Also, the technical support of the Raith-HKUST Nanotechnology Laboratory (project No. SEG\_HKUST08) at MCPF of HKUST is appreciated.

## Compliance with ethical standards

**Conflict of interest** The authors declare that they have no conflict of interest.

## References

- Al Dahoudi N, AlKahlout A, Heusing S et al (2013) Indium doped zinc oxide nanopowders for transparent conducting coatings on glass substrates. *J Sol-Gel Sci Technol* 67:556–564
- Althues H, Henle J, Kaskel S (2007) Functional inorganic nanofillers for transparent polymers. *Chem Soc Rev* 36: 1454–1465

- Becheri A, Durr M, Lo Nostro P et al (2008) Synthesis and characterization of zinc oxide nanoparticles: application to textiles as UV-absorbers. *J Nanopart Res* 10:679–689
- Beena D, Lethy KJ, Vinodkumar R, Mahadevan Pillai VP, Ganesan V, Phase DM, Sudheer SK (2009) Effect of substrate temperature on structural, optical and electrical properties of pulsed laser ablated nanostructured indium oxide films. *Appl Surf Sci* 255:8334–8342
- Chava RK, Kang M (2017) Improving the photovoltaic conversion efficiency of ZnO based dye sensitized solar cells by indium doping. *J Alloys Compd* 692:67–76
- Chen L, Xu J, Holmes JD, Morris MA (2010) A facile route to ZnO nanoparticle superlattices: synthesis, functionalization, and self-assembly. *J Phys Chem C* 114:2003–2011
- Chen M, Wang Z, Han D, Gu F, Guo G (2011) Porous ZnO polygonal nanoflakes: synthesis, use in high-sensitivity NO<sub>2</sub> gas sensor, and proposed mechanism of gas sensing. *J Phys Chem C* 115:12763–12773
- Chen YF, Kim M, Lian G, Johnson MB, Peng X (2005) Side reactions in controlling the quality, yield, and stability of high quality colloidal nanocrystals. *J Am Chem Soc* 127:13331–13337
- Dattoli EN, Lu W (2011) ITO nanowires and nanoparticles for transparent films. *MRS Bull* 36:782–788
- Dou QQ, Ng KM (2016) Synthesis of various metal stearates and the corresponding monodisperse metal oxide nanoparticles. *Powder Technol* 301:949–958
- Hammarberg E, Prodi-Schwab A, Feldmann C (2009) Microwave-assisted polyol synthesis of aluminium- and indium-doped ZnO nanocrystals. *J Colloid Interf Sci* 334: 29–36
- Hansen CM (2007) Hansen solubility parameters: a user's handbook, Second Edition. CRC Press Inc., Boca Raton, Florida
- Jiang C, Cheng MJ, Liu HT, Shao L, Zeng X, Zhang Y, Shi F (2013) Fabricating transparent multilayers with UV and near-IR double-blocking properties through layer-by-layer assembly. *Ind Eng Chem Res* 52:13393–13400
- Khrenov V, Klapper M, Koch M, Müllen K (2005) Surface functionalized ZnO particles designed for the use in transparent nanocomposites. *Macromol Chem Phys* 206:95–101
- Kim GH, Shin HS, Ahn BD, Kim KH, Park WJ, Kim HJ (2009) Formation mechanism of solution-processed nanocrystalline InGaZnO thin film as active channel layer in thin-film transistor. *J Electrochem Soc* 156:H7–H9
- Kirchberg S, Rudolph M, Ziegmann G et al (2012) Nanocomposites based on technical polymers and sterically functionalized soft magnetic magnetite nanoparticles: synthesis, processing, and characterization. *J Nanomater* 2012:8
- Lee JH, Park BO (2003) Transparent conducting ZnO: Al, In and Sn thin films deposited by the sol-gel method. *Thin Solid Films* 426:94–99
- Lee S (2009) Developing UV-protective textiles based on electrospun zinc oxide nanocomposite fibers. *Fibers Polym* 10:295–301
- Li P, Liang Y-H, Ma P-S, Zhu C (1997) Estimations of enthalpies of vaporization of pure compounds at different temperatures by a corresponding-states group-contribution method. *Fluid Phase Equilib* 137:63–74
- Li ST, Qiao XL, Chen HG et al (2006) Effects of temperature on indium tin oxide particles synthesized by co-precipitation. *J Cryst Growth* 289:151–156
- Lizundia E, Ruiz-Rubio L, Vilas JL et al (2016) Poly(L-lactide)/ZnO nanocomposites as efficient UV-shielding coatings for packaging applications. *J Appl Polym Sci* 133:7
- Luo SJ, Feng JY, Ng KM (2014a) Large scale synthesis of nearly monodisperse, variable-shaped In<sub>2</sub>O<sub>3</sub> nanocrystals via a one-pot pyrolysis reaction. *CrystEngComm* 16:9236–9244
- Luo SJ, Feng JY, Ng KM (2015) Effect of fatty acid on the formation of ITO nanocrystals via one-pot pyrolysis reaction. *CrystEngComm* 17:1168–1172
- Luo SJ, Yang DN, Feng JY, Ng KM (2014b) Synthesis and application of non-agglomerated ITO nanocrystals via pyrolysis of indium-tin stearate without using additional organic solvents. *J Nanopart Res* 16:2561
- Luo SJ, Yang DN, Zhuang JL, Ng KM (2013) Synthesis and characterization of nearly monodisperse deltoidal icositrahedral In<sub>2</sub>O<sub>3</sub> nanocrystals via one-pot pyrolysis reaction. *CrystEngComm* 15:8065–8068
- Mahltig B, Botcher H, Rauch K et al (2005) Optimized UV protecting coatings by combination of organic and inorganic UV absorbers. *Thin Solid Films* 485:108–114
- Maldonado A, Olvera MDL, Guerra ST et al (2004) Indium-doped zinc oxide thin films deposited by chemical spray starting from zinc acetylacetonate: effect of the alcohol and substrate temperature. *Sol Energy Mat Sol Cells* 82:75–84
- Morimoto T, Tomonaga H, Mitani A (1999) Ultraviolet ray absorbing coatings on glass for automobiles. *Thin Solid Films* 351:61–65
- Mozaffari S, Li W, Thompson C et al (2017) Colloidal nanoparticle size control: experimental and kinetic modeling investigation of the ligand-metal binding role in controlling the nucleation and growth kinetics. *Nano* 9:13772–13785
- NanoMarkets L (2014) Smart Windows Markets 2014
- Olvera ML, Gómez H, Maldonado A (2007) Doping, vacuum annealing, and thickness effect on the physical properties of zinc oxide films deposited by spray pyrolysis. *Sol Energy Mat Sol Cells* 91:1449–1453
- Raj AME, Lalithambika KC, Vidhya VS et al (2008) Growth mechanism and optoelectronic properties of nanocrystalline In<sub>2</sub>O<sub>3</sub> films prepared by chemical spray pyrolysis of metal-organic precursor. *Physica B* 403:544–554
- Rappe AK, Casewit CJ, Colwell KS, Goddard WA, Skiff WM (1992) UFF, a full periodic table force field for molecular mechanics and molecular dynamics simulations. *J Am Chem Soc* 114:10024–10035
- Rudolph M, Peuker UA (2011) Coagulation and stabilization of sterically functionalized magnetite nanoparticles in an organic solvent with different technical polymers. *J Colloid Interf Sci* 357:292–299
- Shaheen TI, El-Naggar ME, Abdelgawad AM et al (2016) Durable antibacterial and UV protections of in situ synthesized zinc oxide nanoparticles onto cotton fabrics. *Int J Biol Macromol* 83:426–432
- Sirvio JA, Visanko M, Heiskanen JP et al (2016) UV-absorbing cellulose nanocrystals as functional reinforcing fillers in polymer nanocomposite films. *J Mater Chem A* 4:6368–6375
- Sun D, Sue HJ, Miyatake N (2008) Optical properties of ZnO quantum dots in epoxy with controlled dispersion. *J Phys Chem C* 112:16002–16010
- Sunde TOL, Garskaite E, Otter B, Fossheim HE, Sæterli R, Holmestad R, Einarsrud MA, Grande T (2012) Transparent

- and conducting ITO thin films by spin coating of an aqueous precursor solution. *J Mater Chem* 22:15740–15749
- Tao F, Xiaomeng H, Zulan L et al (2016) UV-blocking property of nano-ZnO thin film coating on silk fabric. *Appl Mech Mater* 835:50–54
- Wang QL, Yang YF, He HP, Chen DD, Ye ZZ, Jin YZ (2010) One-step synthesis of monodisperse in-doped ZnO nanocrystals. *Nanoscale Res Lett* 5:882–888
- Wienke J, Booij AS (2008) ZnO: in deposition by spray pyrolysis—influence of the growth conditions on the electrical and optical properties. *Thin Solid Films* 516:4508–4512
- Zayat M, Garcia-Parejo P, Levy D (2007) Preventing UV-light damage of light sensitive materials using a highly protective UV-absorbing coating. *Chem Soc Rev* 36:1270–1281
- Zhang B, Han J (2016) Preparation and UV-protective property of PVAc/ZnO and PVAc/TiO<sub>2</sub> microcapsules/poly(lactic acid) nanocomposites. *Fibers Polym* 17:1849–1857
- Zhao Y, Kong XR, Zeng XF et al (2009) Preparation of ITO nanoparticles and their composite films with infrared property. *J B Univ Chem Technol (Nat Sci Ed)* 36:4–7